Humoral immunogenicity comparison of XBB and JN.1 in human infections

Fanchong Jian[1,2,3,#], Ayijiang Yisimayi[1,2,4,#], Weiliang Song[1,2,4,#], Jing Wang[1,2,4,#], Yanli Xu[5,#], Xiaosu Chen[6], Yuanling Yu[2], Xiao Niu[1,3], Sijie Yang[1,7], Peng Wang[2], Haiyan Sun[2], Lingling Yu[2], Jing Wang[2], Yao Wang[2], Ran An[2], Wenjing Wang[2], Tianhe Xiao[1,8], Qingqing Gu[2], Fei Shao[2], Youchun Wang[2,9], Zhongyang Shen[10], Ronghua Jin[5], Yunlong Cao[1,2,7*]

[1]Biomedical Pioneering Innovation Center (BIOPIC), Peking University, Beijing, China.

[2]Changping Laboratory, Beijing, China.

[3]College of Chemistry and Molecular Engineering, Peking University, Beijing, China.

[4]School of Life Sciences, Peking University, Beijing, China.

[5]Beijing Ditan Hospital, Capital Medical University, Beijing, China.

[6]Institute for Immunology, College of Life Sciences, Nankai University, Tianjin, China.

[7]Peking-Tsinghua Center for Life Sciences, Tsinghua University, Beijing, China.

[8]Joint Graduate Program of Peking-Tsinghua-NIBS, Academy for Advanced Interdisciplinary Studies, Peking University, Beijing, China.

[9]Institute of Medical Biology, Chinese Academy of Medical Science & Peking Union Medical College, Kunming, China.

[10]Organ Transplant Center, NHC Key Laboratory for Critical Care Medicine, Tianjin First Central Hospital, Nankai University, Tianjin, China.

[*]Correspondence: Yunlong Cao (yunlongcao@pku.edu.cn).

[#]These authors contributed equally.

Abstract

The ongoing evolution of SARS-CoV-2 continues to challenge the global immune barrier established by infections and vaccine boosters. Recently, the emergence and dominance of the JN.1 lineage over XBB variants have prompted a reevaluation of current vaccine strategies. Despite the demonstrated effectiveness of XBB-based vaccines against JN.1, concerns persist regarding the durability of neutralizing antibody (NAb) responses against evolving JN.1 subvariants. In this study, we compared the humoral immunogenicity of XBB and JN.1 lineage infections in human subjects with diverse immune histories to understand the antigenic and immunogenic distinctions between these variants. Similar to observations in naïve mice, priming with XBB and JN.1 in humans without prior SARS-CoV-2 exposure results in distinct NAb responses, exhibiting minimal cross-reactivity. Importantly, breakthrough infections (BTI) with the JN.1 lineage induce 5.9-fold higher neutralization titers against JN.1 compared to those induced by XBB BTI. We also observed notable immune evasion of recently emerged JN.1 sublineages, including JN.1+R346T+F456L, with KP.3 showing the most pronounced decrease in neutralization titers by both XBB and JN.1 BTI sera. These results underscore the challenge posed by the continuously evolving SARS-CoV-2 JN.1 and support the consideration of switching the focus of future SARS-CoV-2 vaccine updates to the JN.1 lineage.

Main

Since the emergence of the SARS-CoV-2 BA.2.86 lineage in July 2023, its subvariants, especially JN.1, have continued to circulate and evolve rapidly, outcompeting the previously prevalent XBB subvariants [1,2]. By March 2024, the JN.1 lineage accounted for over 93% of newly observed sequences (Extended Data Fig. 1a).

BA.2.86 and JN.1 have convergently accumulated mutations on the receptor-binding domain (RBD) of the viral spike glycoprotein, including R346S/T, F456L/V, and A475V/S (Extended Data Fig. 1b). These subvariants, represented by JN.1+R346T (such as JN.1.18, JN.1.13.1, and JN.1.24), JN.1+F456L (such as JN.1.16 and JN.1.11.1), and their combination, JN.1+R346T+F456L (so-called "FLiRT" variants), exhibit a remarkable growth advantage during their recent circulation (Extended Data Fig. 1a-b). A newly detected subvariant, designated as KP.3, even carries a Q493E mutation, likely exhibiting distinct behaviors compared to the previously well-known Q493R, whose reversion increases the receptor-binding affinity [3]. Most of these sites mutated in JN.1 subvariants are located near the receptor-binding motif (RBM) and are known to be related to antibody escape (Extended Data Fig. 1c). This makes it crucial to investigate their capabilities of evading the current immune barrier established by SARS-CoV-2 infections and vaccines.

Previous studies demonstrated the satisfactory capability of eliciting JN.1-effective neutralizing antibodies of the currently recommended XBB-based vaccine boosters [4,5]. However, it is important to investigate whether JN.1 immunization performs substantially better against these novel subvariants than XBB. Here in this manuscript, we systematically compared the humoral immune response of XBB* and JN.1 in human infections and mice vaccination against JN.1 sublineages. Results suggest that future SARS-CoV-2 vaccine efforts might benefit from focusing on the JN.1 lineage instead of XBB to better counter current and emerging variants.

Results

We collected plasma samples from seven cohorts, including individuals infected by XBB* (n=11) or JN.1 (n=4) without known previous exposure to SARS-CoV-2, those who experienced sequential infections of BA.5/BF.7 and XBB* (n=14), or BA.5/BF.7 and JN.1 (n=29), and those who received

3-dose inactivated vaccines followed by BA.5/BF.7 breakthrough infection (BTI) and then reinfected by XBB (mainly XBB+S486P), HK.3, or JN.1 (n=54, 18, 29, respectively) (Fig. 1a). Infection strains were inferred based on the sampling time when the corresponding strain was the majority of detected sequences in the region of sample collection. SARS-CoV-2 Infection was confirmed by either antigen or PCR tests.

Priming with XBB and JN.1 in humans elicited distinct neutralizing antibodies without observable cross-lineage reactivity (Fig. 1b). Such distinct antigenicity between XBB and JN.1 was also confirmed in mice, showing remarkable antigenic distances between these lineages (Extended Data Fig. 2a-c). In contrast, a prior BA.5 or BF.7 infection improved the cross-lineage reactivity of antibodies induced by XBB or JN.1 reinfection. This suggests that BA.5/BF.7 priming could induce Omicron cross-reactive neutralizing antibodies that are effective against both XBB and JN.1 lineages (Fig. 1c).

In the three BTI with reinfection cohorts, "BA.5/BF.7 BTI + XBB" elicited the lowest NT_{50} against JN.1 lineage variants (Fig. 1d). On average, JN.1 reinfection induced a 5.9-fold higher NT_{50} against JN.1, and a 4.7-fold higher NT_{50} against JN.1+R346T+F456L ("FLiRT"), compared with XBB reinfection (Fig. 1e). The improvement of JN.1 BTI over HK.3 BTI was less significant, possibly due to the shorter interval between infections in the XBB cohort and the immunogenicity drift from HK.3's "FLip" mutation.

Among all five reinfection cohorts, all of the four JN.1 subvariants tested, including JN.1+R346T, JN.1+F456L, JN.1+R346T+F456L, and KP.3, exhibited notable immune evasion. KP.3 consistently acted as the strongest escaper, leading to a 1.9 to 2.4-fold reduction in NT50 compared to JN.1, likely due to the unprecedented Q493E mutation of KP.3.

Antigenic cartography of our plasma neutralization data visualized the antigenic differences of SARS-CoV-2 variants. The antigenic map from single-exposure cohorts clearly depicted the intrinsic antigenic distances between XBB and JN.1 lineage, despite sample size limitations (Fig. 1f). Samples from BTI with reinfection cohorts showed strong ancestral strain imprinting, indicated by the aggregation of points near the D614G strain (Fig. 1g). Nevertheless, the JN.1 BTI cohorts displayed closer distance to current circulating variants, supporting the idea of switching vaccine

boosters to JN.1 lineages.

Previous studies have highlighted the synergistic impact of RBD L455-F456 mutations on ACE2 receptor binding affinity [6]. Given these sites are also convergently mutated in BA.2.86 lineages (especially JN.1), we tested the binding affinities of JN.1 subvariant RBD to human ACE2 (hACE2) using surface plasmon resonance (SPR). Interestingly, F456L (K_D=12 nM) and R346T+F456L (K_D=11 nM) did not largely affect the hACE2-binding affinity of JN.1 (K_D=13 nM), indicating that unlike L455F in HK.3, the dampened ACE2 affinity of JN.1 due to L455S could not be compensated by F456L. Notably, another JN.1 subvariant designated as JN.1.23, which harbors K444R+Y453F mutation, showed substantially higher affinity to ACE2, potentially allowing for more immune evasive mutations in the future (Extended Data Fig. 3).

Together, our results underscore the significant antigenic distinctions between the SARS-CoV-2 XBB and JN.1 lineages and provide compelling evidence to shift the focus of vaccine booster strategies from XBB to the JN.1 lineage. Despite the notable cross-lineage reactivity elicited by XBB as a booster, boosters based on JN.1 may offer superior protection against current and forthcoming JN.1 subvariants. Furthermore, the ongoing evolution of JN.1 subvariants, particularly those with enhanced receptor-binding capabilities, warrants vigilant monitoring.

Acknowledgments

This project is financially supported by the Ministry of Science and Technology of China (2023YFC3043200), Changping Laboratory (2021A0201; 2021D0102), and National Natural Science Foundation of China (32222030).

Declaration of interests

Y.C. is a co-founder of Singlomics Biopharmaceuticals. Other authors declare no competing interests.

Figure legend

Figure 1 | Antigenicity and immunogenicity comparison of XBB and JN.1 lineages

a, Schematic of the SARS-CoV-2-related immune histories of the seven cohorts involved in this study. **b-d**, 50% neutralization titers (NT_{50}) of plasma samples from seven different cohorts against SARS-CoV-2 variant pseudoviruses. Plasma source cohorts and corresponding number of samples are labeled above each panel. Dashed line indicates limit of detection (NT_{50} = 10). Numbers of negative samples are labeled below the dashed lines. Geometric mean titers (GMT) values are labeled as black bars and shown above each group of points, with fold-changes and significance compared to JN.1 labeled. Wilcoxon signed-rank tests are used to calculate the p-values. **e**, Comparison of neutralization of plasma samples from three BTI+reinfection cohorts against JN.1 and JN.1+R346T+F456L. GMT values are labeled as black bars and above the points, with pair-wise fold-changes shown. Wilcoxon rank-sum tests are used to determined the p-values. *p<0.05; **p<0.01; ***p<0.001; ****p<0.0001; NS, not significant. **f-g**, Antigenic cartography performed using human plasma neutralization data of single-exposure cohorts (**f**) or ancestral strain imprinted cohorts (**g**). Each square indicates a plasma sample and each circle indicates a SARS-CoV-2 variant.

Extended Data Figure legend

Extended Data Fig. 1 | Prevalence convergent evolution of JN.1 lineage

a, Dynamics of the percentage of XBB and JN.1 lineages in GISAID sequences from Sept 2023 to Apr 2024. **b**, Schematic for the convergent evolution of BA.2.86/JN.1 lineage. **c**, Key mutated sites of BA.2.86/JN.1 lineage are indicated on the XBB.1.5 RBD structural model (PDB: 8WRL).

Extended Data Fig. 2 | Distinct antigenicity of XBB and JN.1 in mice

a, Schematic for the mouse immunization experiments. **b**, Antigenic cartography of mouse sera neutralization data. Each square indicates a plasma sample and each circle indicates a SARS-CoV-2 variant. **c**, Serum NT_{50} of mouse that received 2-dose WT, BA.5, XBB.1.5, or JN.1 Spike mRNA vaccine against eight representative SARS-CoV-2 variants.

Extended Data Fig. 3 | ACE2-binding affinity of variant RBD

Barplots show the affinities of SARS-CoV-2 variants, including WT, BA.5, BQ.1.1, in addition to XBB and BA.2.86 subvariants, determined by SPR. Each circle indicate a replicate. Geometric

mean K_D (nM) values are annoateted above each bar.

Methods

Plasma isolation

Blood samples were collected from individuals who had either recovered from or been re-infected with the SARS-CoV-2 Omicron BTI variant. This was conducted under the research protocol approved by the Beijing Ditan Hospital, affiliated with Capital Medical University (Ethics Committee Archiving No. LL-2021-024-02), the Tianjin Municipal Health Commission, and the Ethics Committee of Tianjin First Central Hospital (Ethics Committee Archiving No. 2022N045KY). All participants provided their agreement for the collection, storage, and use of their blood samples strictly for research purposes and the subsequent publication of related data.

Patients in the re-infection group were initially infected with the BA.5/BF.7 variants in December 2022 in Beijing and Tianjin, China [7]. From December 1, 2022, to February 1, 2023, over 98% of the sequenced samples were identified as BA.5* (excluding BQ*), primarily consisting of the subtypes BA.5.2.48* and BF.7.14*, which were representative of the BA.5/BF.7 variants during this period. Subsequently, patients in the XBB BTI cohort and those with secondary infections in the re-infection group contracted the virus between May and June 2023. More than 90% of the sequenced samples from Beijing and Tianjin during this period corresponded to the XBB*+486P variant. These infections were confirmed using polymerase chain reaction (PCR) or antigen testing.

Whole blood was diluted in a 1:1 ratio with a solution of phosphate-buffered saline (PBS) supplemented with 2% fetal bovine serum (FBS). This was followed by Ficoll gradient centrifugation (Cytiva, 17-1440-03). After centrifugation, the plasma was collected from the upper layer, stored in aliquots at 20°C or lower, and heat-inactivated prior to subsequent experiments.

Pseudovirus preparation and neutralization

The SARS-CoV-2 spike protein pseudovirus was generated using the vesicular stomatitis virus (VSV) pseudovirus packaging system as described previously [8,9]. The spike protein gene was codon-optimized and integrated into the pcDNA3.1 expression plasmid via the BamHI and XbaI restriction

enzyme sites to augment the expression efficiency of the spike protein in mammalian cells. During pseudovirus production, the 293T cells (American Type Culture Collection (ATCC, CRL-3216)) were transfected with the SARS-CoV-2 spike protein expression plasmid. Post-transfection, these cells were infected with the G*ΔG-VSV virus (VSV-G pseudotyped virus, Kerafast) present in the cell culture supernatant. The pseudovirus was subsequently harvested and filtered from the supernatant, aliquoted, and stored at -80°C for later use.

Pseudovirus neutralization assays were performed using the Huh-7 cell line (Japan Collection of Research Bioresources [JCRB], 0403). Plasma samples were serially diluted and mixed with the pseudovirus. Following an incubation period of 1 hour at 37°C with 5% CO_2, digested Huh-7 cells were introduced and incubated for an additional 24 hours at 37°C. The supernatant was then removed, and the mixture was incubated with D-Luciferin reagent (PerkinElmer, 6066769) in darkness for 2 minutes. The cell lysate was transferred to a detection plate, and the luminescence intensity was measured using a microplate spectrophotometer (PerkinElmer, HH3400). NT_{50} values were determined using a four-parameter logistic regression model [10].

Surface plasmon resonance

SPR experiments were conducted on Biacore 8K (Cytiva) to determine the RBD-hACE2 binding affinities. Human ACE2-Fc was immobilized onto Protein A sensor chips (Cytiva). Purified SARS-CoV-2 variant RBD samples prepared in serial dilutions (6.25, 12.5, 25, 50, and 100 nM) were injected on the sensor chips. Response units were recorded by Biacore 8K Evaluation Software 3.0 (Cytiva) at room temperature. Raw response data were fitted to 1:1 binding models to determine the association and dissociation kinetic constants (k_a and k_d), and binding affinities (dissociation equilibrium constant KD) using Biacore 8K Evaluation Software 3.0 (Cytiva).

mRNA vaccine preparation and mouse immunization

For mRNA vaccine preparation, 5′ untranslated region (UTR), target sequence, and 3′ UTR were sequentially integrated downstream of the T7 promoter within an empty PSP73 plasmid. Subsequently, a double-digestion process was employed to produce linearized DNA. This DNA served as a template for a T7 RNA polymerase-driven in vitro transcription process to generate RNA

that encodes the SARS-CoV-2 S6P (F817P, A892P, A899P, A942P, K986P, V987P, R683A, and R685A) protein, according to the manufacturer's instructions (Vazyme, DD4201). The transcriptional outputs underwent DNase I treatment for the elimination of DNA templates, followed by a purification step utilizing VAHTS RNA Clean Beads (Vazyme, N412-02). Cap 1 structure was added using Vaccinia Capping Enzyme (Vazyme, DD4109) and mRNA Cap 2′-O-methyltransferase (Vazyme, DD4110), with a subsequent purification via magnetic beads. The incorporation of Poly(A) tails was achieved with Escherichia coli Poly(A) Polymerase (Vazyme, N4111-02), culminating in another round of purification.

The mRNA was encapsulated in a functionalized lipid nanoparticle as described previously [11]. Concisely, a solution containing ionizable lipid, DSPC, cholesterol, and PEG2000-DMG was prepared in ethanol, maintaining a molar ratio of 50:10:38.5:1.5, respectively. The mRNA was then diluted in a 50 mM citrate buffer (pH 4.0), free of RNase, to achieve a final lipid:mRNA weight ratio of 6:1. The aqueous and ethanol solutions were mixed in a 3:1 volume ratio using a microfluidic apparatus and the obtained lipid nanoparticles were then subjected to overnight dialysis. To preserve the chemical stability of the components, all samples were stored at temperatures ranging from 2 to 8 °C for up to a week. The dimensions and distribution of particle sizes of the lipid nanoparticles, as well as the encapsulation efficiency and concentration of mRNA, were meticulously assessed, revealing encapsulation rates typically between 90% and 99%.

Animal experiments were carried out under study protocols approved by Rodent Experimental Animal Management Committee of Institute of Biophysics, Chinese Academy of Sciences (SYXK2023300) and Animal Welfare Ethics Committee of HFK Biologics (HFK-AP-20210930). Female BALB/c mice, aged between six to eight weeks, were used for experiments. The mice were housed under a 12-hour light and 12-hour dark cycle, with room temperatures maintained between 20 °C and 26 °C and humidity levels maintained between 30% and 70%. mRNA vaccines were given intramuscularly at dosages of either 10 μg per mouse. Blood samples were collected 2 weeks after the final immunization, as shown in Extended Data Fig. 3a.

References

1 Yang, S. *et al.* Fast evolution of SARS-CoV-2 BA.2.86 to JN.1 under heavy immune pressure.

Lancet Infect Dis (2023). https://doi.org:10.1016/S1473-3099(23)00744-2

2 Kaku, Y. *et al.* Virological characteristics of the SARS-CoV-2 JN.1 variant. *Lancet Infect Dis* (2024). https://doi.org:10.1016/S1473-3099(23)00813-7

3 Starr, T. N. *et al.* Deep mutational scans for ACE2 binding, RBD expression, and antibody escape in the SARS-CoV-2 Omicron BA.1 and BA.2 receptor-binding domains. *PLOS Pathogens* **18**, e1010951 (2022). https://doi.org:10.1371/journal.ppat.1010951

4 Wang, Q. *et al.* XBB.1.5 monovalent mRNA vaccine booster elicits robust neutralizing antibodies against XBB subvariants and JN.1. *Cell Host & Microbe* **32**, 315-321.e313 (2024). https://doi.org:10.1016/j.chom.2024.01.014

5 Jain, S. *et al.* XBB.1.5 monovalent booster improves antibody binding and neutralization against emerging SARS-CoV-2 Omicron variants. *bioRxiv*, 2024.2002.2003.578771 (2024). https://doi.org:10.1101/2024.02.03.578771

6 Jian, F. *et al.* Convergent evolution of SARS-CoV-2 XBB lineages on receptor-binding domain 455–456 synergistically enhances antibody evasion and ACE2 binding. *PLOS Pathogens* **19**, e1011868 (2023). https://doi.org:10.1371/journal.ppat.1011868

7 Pan, Y. *et al.* Characterisation of SARS-CoV-2 variants in Beijing during 2022: an epidemiological and phylogenetic analysis. *The Lancet* **401**, 664-672 (2023). https://doi.org:10.1016/S0140-6736(23)00129-0

8 Li, Q. *et al.* The Impact of Mutations in SARS-CoV-2 Spike on Viral Infectivity and Antigenicity. *Cell* **182**, 1284-1294.e1289 (2020). https://doi.org:10.1016/j.cell.2020.07.012

9 Yisimayi, A. *et al.* Repeated Omicron exposures override ancestral SARS-CoV-2 immune imprinting. *Nature* **625**, 148-156 (2024). https://doi.org:10.1038/s41586-023-06753-7

10 Nie, J. *et al.* Establishment and validation of a pseudovirus neutralization assay for SARS-CoV-2. *Emerg Microbes Infect* **9**, 680-686 (2020). https://doi.org:10.1080/22221751.2020.1743767

11 Yanez Arteta, M. *et al.* Successful reprogramming of cellular protein production through mRNA delivered by functionalized lipid nanoparticles. *Proceedings of the National Academy of Sciences* **115**, E3351-E3360 (2018). https://doi.org:doi:10.1073/pnas.1720542115

Figure 1

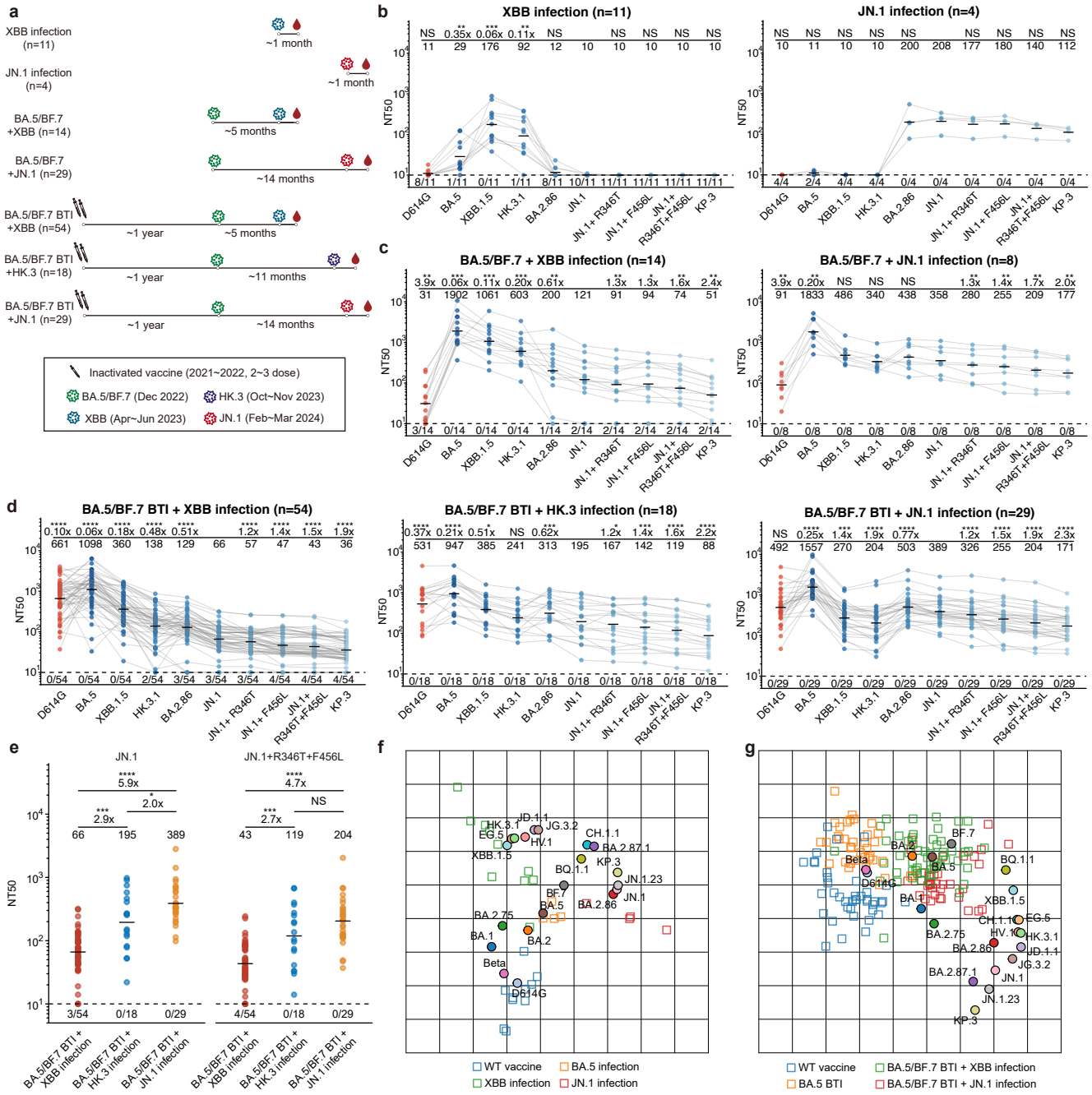
a
XBB infection (n=11)
~1 month
JN.1 infection (n=4)
~1 month
BA.5/BF.7 +XBB (n=14)
~5 months
BA.5/BF.7 +JN.1 (n=29)
~14 months
BA.5/BF.7 BTI +XBB (n=54)
~1 year
~5 months
BA.5/BF.7 BTI +HK.3 (n=18)
~1 year
~11 months
BA.5/BF.7 BTI +JN.1 (n=29)
~1 year
~14 months
Inactivated vaccine (2021~2022, 2~3 dose)
BA.5/BF.7 (Dec 2022)
HK.3 (Oct~Nov 2023)
XBB (Apr~Jun 2023)
JN.1 (Feb~Mar 2024)
b
XBB infection (n=11)
JN.1 infection (n=4)
c
BA.5/BF.7 + XBB infection (n=14)
BA.5/BF.7 + JN.1 infection (n=8)
d
BA.5/BF.7 BTI + XBB infection (n=54)
BA.5/BF.7 BTI + HK.3 infection (n=18)
BA.5/BF.7 BTI + JN.1 infection (n=29)
NT50
D614G
BA.5
XBB.1.5
HK.3.1
BA.2.86
JN.1
JN.1+ R346T
JN.1+ F456L
JN.1+ R346T+F456L
KP.3
e
JN.1
JN.1+R346T+F456L
BA.5/BF.7 BTI + XBB infection
BA.5/BF.7 BTI + HK.3 infection
BA.5/BF.7 BTI + JN.1 infection
f
WT vaccine
BA.5 infection
XBB infection
JN.1 infection
g
WT vaccine
BA.5 BTI
BA.5/BF.7 BTI + XBB infection
BA.5/BF.7 BTI + JN.1 infection

Extended Data Fig. 1

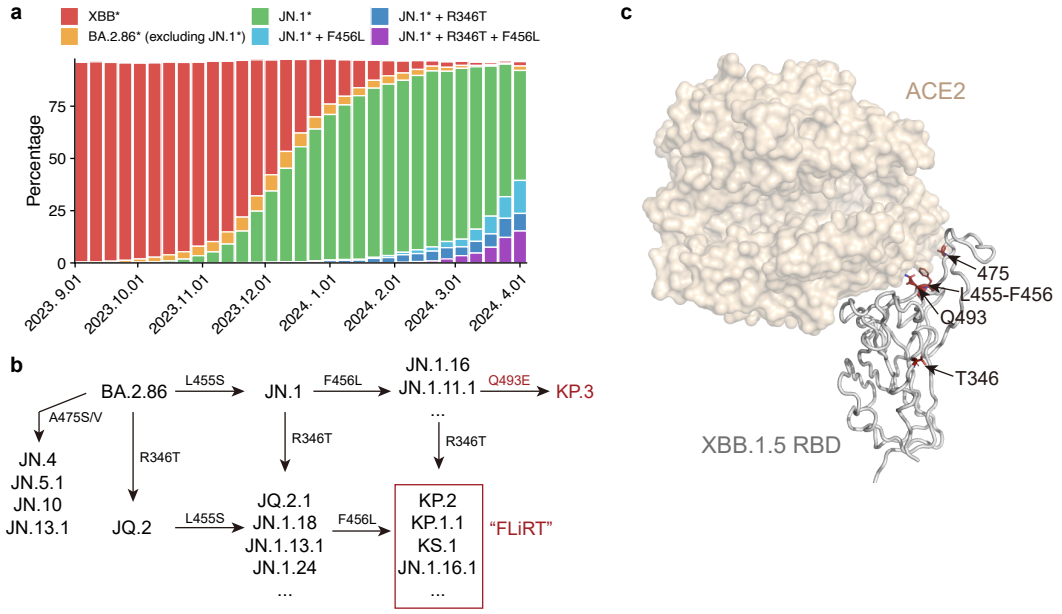

Extended Data Fig. 2

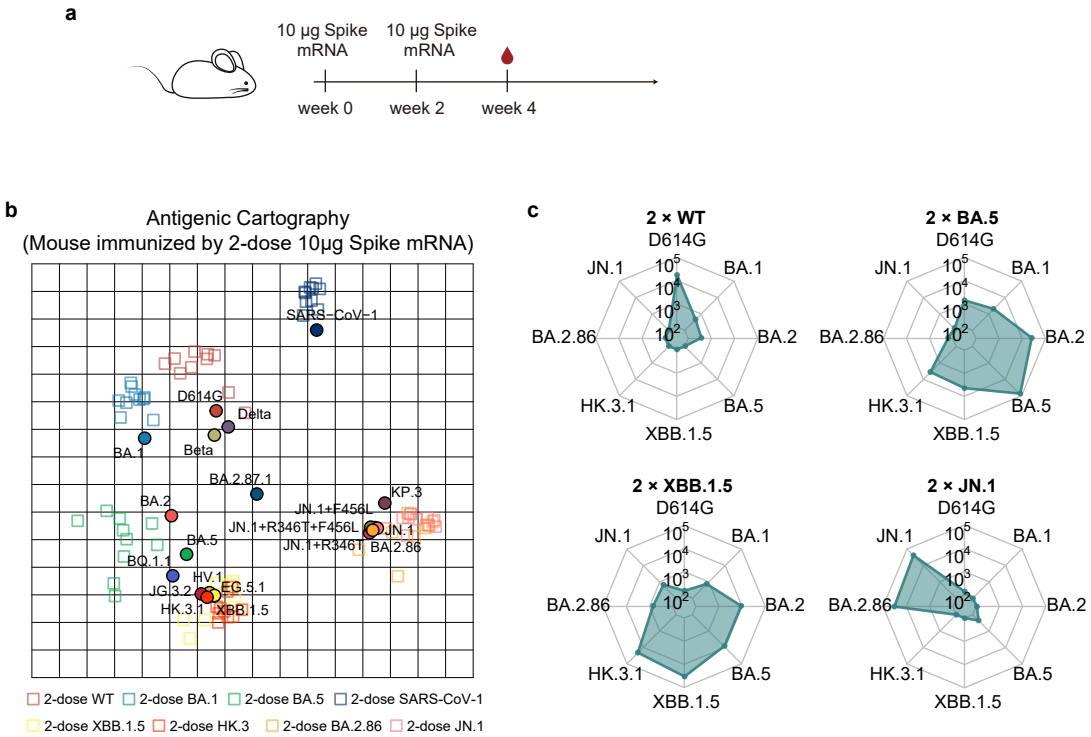
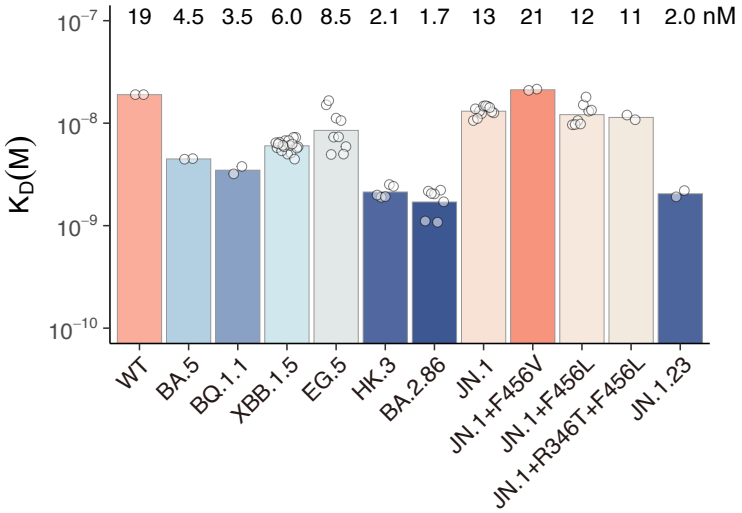
Extended Data Fig. 3